doi:10.14311/ppt.2017.3.249
Plasma Physics and Technology **4**(3):249–252, 2017

EMISSION SPECTROSCOPY DURING HIGH-CURRENT ANODE MODES IN VACUUM ARC

A. Khakpour*, R. Methling, St. Franke, S. Gortschakow, D. Uhrlandt

Leibniz-Institut for Plasma Science and Technology, Felix-Hausdorff-Str. 2, 17489 Greifswald, Germany

* alireza.khakpour@inp-greifswald.de

Abstract. A vacuum interrupter reaches its interruption limit once high-current anode phenomena occur. High-current anode modes lead to an increase of the anode surface temperature and an increased generation of metal vapor, which may result in a weakening of the dielectric recovery strength after current zero. In this work, different discharge modes in a vacuum arc for AC 50 Hz including diffuse, footpoint, anode spot type 1 and type 2, and anode plume are investigated. Electrodes made of CuCr7525 with diameter of 10 mm are used. The final gap length is about 20 mm. Time and space resolved optical emission spectroscopy is used to examine the temporal and spatial distribution of atomic and ionic copper lines. The distribution of atomic and ionic lines parallel and perpendicular to the anode surface is investigated. Radiator density is also determined for Cu I, Cu II, and Cu III near the anode surface.

Keywords: vacuum arc, high-current anode phenomena, emission spectroscopy.

1. Introduction

The interest in developing vacuum circuit breakers for high-voltage applications is still growing, whereas the high-current anode phenomena are important due to their impact on the contact erosion and interruption failure [1, 2]. Different high-current anode modes including footpoint, anode spot type 1 and type 2, and intense mode in which the anode plays an active role are investigated in [3]. The transition from the low-current mode to high-current modes is associated with considerable changes in the optical, thermal, and electrical properties near to the anode, the cathode, and in the inter-electrode gap [4, 5].

Different discharge modes have been investigated by means of the evaluation of high-speed camera images and electrical characteristics [5]. The temporal and axial distribution of different atomic and ionic lines during transition between different discharge modes are investigated in [4]. Two types of anode spot modes are investigated in [5] which differ in the voltage course and the radiation intensity. The anode spot type 2 appears at higher gap length and even lower current comparing to anode spot type 1. An abrupt change in the arc voltage and intensity of Cu I–III lines is observed during transition to anode spot type 2. However, the previous work is focused on the axial distribution of line intensity of different copper species. Nevertheless, more information regarding different discharge modes in vacuum arc and recent research can be find in [6].

In this work the temporal distribution of Cu I, Cu II, and Cu III lines is examined near the anode for AC 50 Hz during transition between different high-current anode modes. Temporal and spatial distribution of radiating density is presented for different high-current anode modes.

2. Experimental setup

The schematic representation of the experimental setup is discussed in [4]. The power source consists of capacitors, inductances, charging and control units and enables the possibility to realize different current waveforms. In the present work a sinusoidal alternating current at 50 Hz is used. To generate an AC 50 Hz waveform, five LC elements are applied in parallel. The capacitance and inductance of each branch is 512 µF and 4700 µH, respectively. This part is in series with inductance of 2730 µH. Different current levels can be achieved by adjusting the charging voltage of the capacitors.

The ultrahigh vacuum chamber with basic pressure of about 2×10^{-8} mbar is equipped with mounting adapters for different electrodes. In this work, cylindrical electrodes of CuCr7525 with a diameter of 10 mm are used. A mechanical-pneumatic actuator system is designed for the separation of electrodes. The upper electrode is fixed and connected to the power supply, whereas the lower electrode can be moved down. Constant opening velocities are obtained that can be chosen between 1 m/s to 4 m/s depending on the starting pressure in the actuator. The maximum gap length is about 20 mm. The delay between start of current and electrode separation can be adjusted freely with a total jitter below 100 µs [4]. So, the arc voltage is appears at the moment of the opening the contacts.

The registration of the arc dynamics and observation of anode modes is realized by means of a high-

speed video camera (Y4 series from Integrated Design Tools) with a recording speed of 20 000 fps. The spectroscopic setup consists of an imaging spectrograph with 0.5 m focal length (SP2500 from Princeton Instruments) combined with high-speed camera (IDT Y4) with a recording speed of 10 000 frames per second. Usually, that technique is named as video spectroscopy. In our case, it enables to study the temporal evolution of lines of different atoms and ions including their spatial profiles during one pulse with 100 µm resolution. Therefore, it is appropriate also for cases of limited reproducibility. The area at a distance of 1.0 mm to the anode is imaged to the entrance slit of the spectrograph using an entrance slit width of 50 µm and grating with 150 lines per mm.

For registration of electrical signals a system consisting of a Pearson current monitor (Model 1423) is used with a resistance of 1 mΩ and with low and high frequency 3 dB cut-off of 1 Hz and 1.2 MHz, respectively. To measure the voltage, a voltage probe (Tektronix 6015A) with a bandwidth of 75 MHz is used.

3. Experimental results

Experiments have been performed applying AC waveforms and peak currents of up to 4.5 kA. Contact separation speed has been set to 1.2 m/s and the final gap distance was 20 mm. The successive transition from the diffuse to the different high-current anode modes is illustrated in the following by current and voltage waveforms together with high-speed camera images. The time behavior of Cu atomic and ionic lines is investigated in cases parallel and perpendicular to the anode surface.

3.1. Electrical characteristics and high-speed camera images

Fig. 1 presents the formation of different discharge modes of the vacuum arc including diffuse, footpoint mode, anode spot type 1, anode spot type 2, and anode plume for AC 50 Hz. The corresponding current and voltage traces are presented in Fig. 2. The opening time is about 0.40 ms and the maximum current about 4.4 kA in this example.

At the beginning of the discharge, a diffuse mode can be observed (Fig. 1a), after that the footpoint mode appears until 3.6 ms when anode spot type 1 occurs (Fig. 1b). Anode spot type 1 continues up to 5.4 ms. Notice, with the transition to anode spot type 1 at about 3.6 ms, the average of the arc voltage jumps up by about 10 % (Fig. 2). Then anode spot type 2 appears corresponding to brighter illumination areas at both anode and cathode compared to anode spot type 1 (cf. Fig. 1c to f). As presented in Fig. 2 the transition to anode spot type 2 is associated with the abrupt change in the arc voltage of about 35 %. After extinction of anode spot type 2 (Fig. 1g) the anode plume appears on the anode (Fig. 1f) and it continues up to the extinction of the arc.

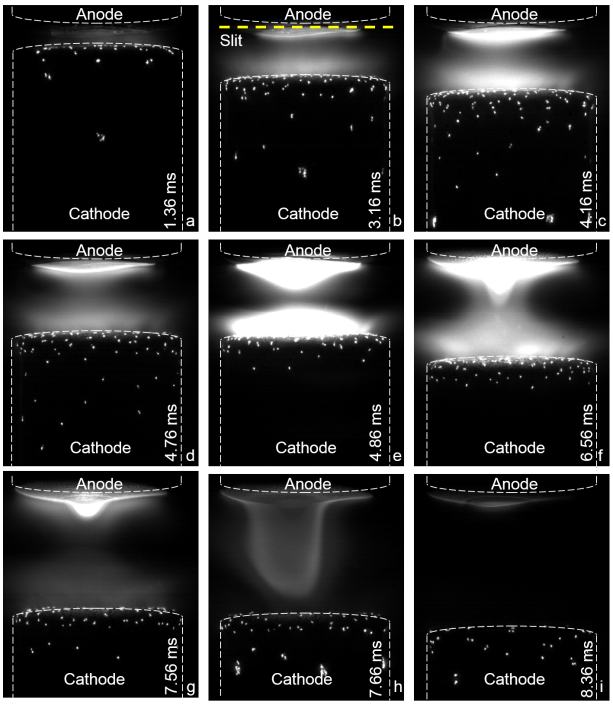

Figure 1. The formation of different discharge modes: diffuse (a), footpoint (b), anode spot type 1 (c and d), anode spot type 2 (e, f. and g), anode plume (h), and diffuse (i).

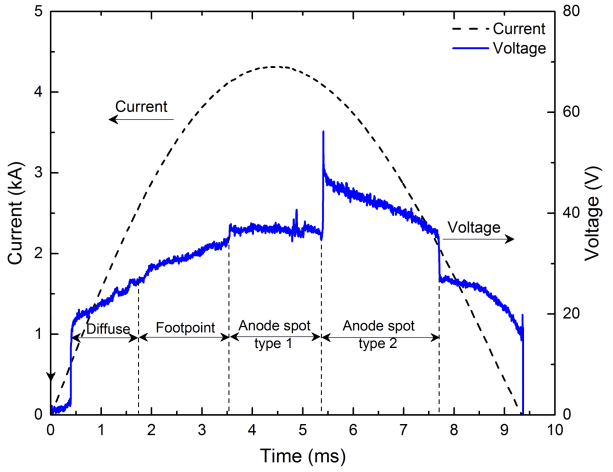

Figure 2. The current and voltage waveforms during transition to different anode spot modes. The time instant of the formation of different high-current anode modes are presented.

3.2. Spectroscopy parallel to the anode surface

To get information about distribution of atomic and ionic line radiation during the anode spot modes the spectrograph has been aligned parallel to the anode surface at a distance of 1.0 mm from the anode surface (cf. dotted line in Fig. 1b). The spectral range 440−580 nm is chosen that contains well-resolved spectral lines of different ionization states of Cu and Cr. The local emission coefficients of the Cu I lines can be estimated based on Abel inversion of parts of the line

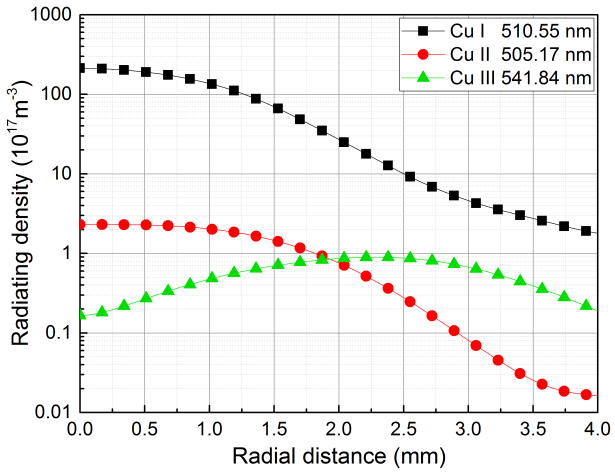

Figure 3. The density of radiating species of Cu I [510.55 nm], Cu II [505.17 nm] and Cu III [541.84 nm] during anode spot type 1 at 4.5 ms and at a distance of 1.0 mm from anode surface in dependence on the distance from the anode spot center.

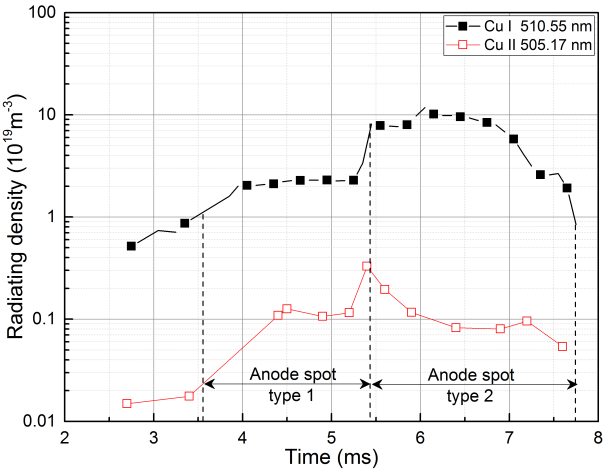

Figure 4. The temporal distribution of the radiating density for Cu I [510.55 nm] and Cu II [505.17 nm]in the anode spot center and at a distance of 1.0 mm from anode surface.

integrated Cu I radiation after absolute calibration of the measured intensities. The local emission coefficient ε of a transition from an upper level u to a lower level l is related to the local radiating density n_u, i.e. the density of excited Cu atoms of the corresponding upper level u can be calculated according to

$$\varepsilon = \frac{1}{4\pi}\frac{hc}{\lambda} n_\mathrm{u} A_\mathrm{lu} \qquad (1)$$

where λ is the transition line wavelength, A_{ul} is the transition probability, h is the Planck constant, and c is the speed of light. Results for the upper level excited state densities corresponding to the lines Cu I [510.55 nm], Cu II [505.17 nm] and Cu III [541.84 nm] during anode spot type 1 (at 4.5 ms after contact opening) are presented in Fig. 3.

The radiating density of Cu I at 510.55 nm at the center of anode spot type 1 is about 2×10^{19} m^{-3}, whereas the density of radiating species of Cu II at 493.16 nm and Cu III at 541.84 nm are about 2×10^{17} m^{-3} and 2×10^{16} m^{-3}, respectively. Notice, outside the anode spot at about 2 mm the radiating density of Cu III is higher than Cu II which can be also confirmed by different intensity distribution of anode spot.

The temporal distribution of the radiating density of Cu I [510.55 nm] at the center of anode spot and a distance of 1.0 mm from anode surface is presented in Fig. 4. During footpoint mode the radiating density is in the range of $5 - 7 \times 10^{18}$ m^{-3}. During anode spot type 1 the radiating density is about $1 - 2 \times 10^{19}$ m^{-3}. After transition to the anode spot type 2 at 5.4 ms, the radiating density is about 9×10^{19} m^{-3} and it starts to decrease at 6.5 ms. After extinction of the anode spot type 2 at 7.7 ms, the radiating density decreases strongly. Notice that the radiating density for the time instant before 2.5 ms is not presented due to the weak emission lines.

Notice, that conclusions from the radiating densities to ground state densities of atoms and ions are not possible without knowledge of additional physical quantities because of the non-equilibrium nature of the vacuum arc plasma.

3.3. Spectroscopy perpendicular to the anode surface

The axial intensity distribution of atomic and double charge ion lines are selected here for comparison. The spectrograph has been aligned for an observation along a line perpendicular to the anode surface at the center of the electrodes. The axial distributions during the transition from the diffuse mode to high-current anode modes including footpoint mode, anode spot type 1 and 2 are presented in Fig. 5. The approximate positions of anode and cathode are also presented using the high-speed camera images. The intensity of each species is normalized with respect to the peak intensity of anode spot type 2.

The relative intensity of the Cu I line near to the anode becomes larger with each anode mode. Cu I line intensity shows a pronounced decrease towards the cathode. Notice, the distribution of Cu I line in case of anode spot type 2 is broader compared to other discharge modes which is in a good agreement with the radiation intensity of anode spot type 2 presented in Fig. 1. In different discharge modes, the intensity of the Cu I line changes slightly near the cathode.

The relative intensities of the Cu II line during footpoint mode and anode spot modes are similar to those of the Cu I line near to the anode and the cathode. Note, that a graphic illustration is omitted here for the sake of brevity. However, the profile near to the anode is much broader compared to the Cu I line. Notice, in case of diffuse mode the intensity of the Cu II line near to the anode is very low.

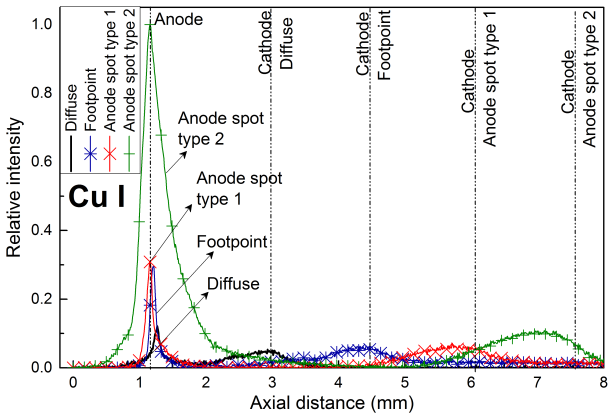

Figure 5. Axial intensity distributions of the line Cu I [510.55 nm] during transition from diffuse mode to different high-current anode modes. The dashed lines correspond to the corresponding electrode positions.

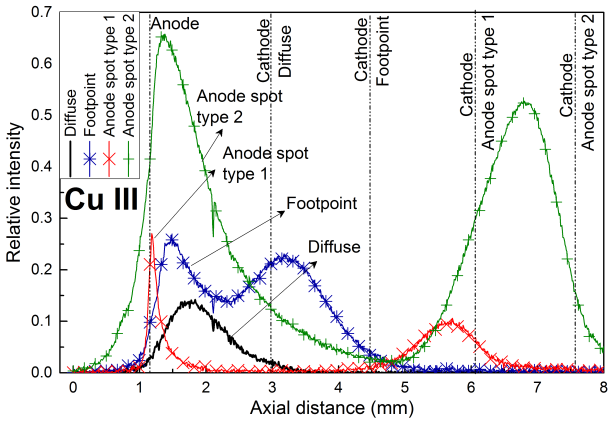

Figure 6. Axial intensity distribution of the line Cu III [509.42 nm] during transition from diffuse mode to different high-current anode modes. The dashed lines correspond to the corresponding electrode positions.

The relative intensity of the Cu III line shows a different behavior than Cu I with a much broader spatial profile along the discharge axis. There is a clear change in the distribution of the Cu III line during transition from diffuse mode to footpoint mode and anode spot modes near the anode, the cathode and in the inter-electrode gap. It seems that the intensity of the Cu III line has also two maxima near to the anode and the cathode but more distant from the surfaces compared to Cu I. The two maxima cannot be resolved in the diffuse mode and are still overlapping in the footpoint mode. The line intensity of Cu III in case of footpoint mode and anode spot type 1 mode is almost the same near the anode.

However, the intensity near the cathode is higher in case of footpoint mode. During anode spot type 2 the intensity of the Cu III line increases near to the anode and cathode and has a much broader profile there comparing to anode spot type 1.

The high intensity of the Cu III line near the anode during anode spot of both types give strong hint that double charged Cu ions near the anode originate from the plasma emitted from the anode.

The absolute error can be estimated to 20-30 % for both intensity and density of radiating species. Relative errors influencing the shape of the profile can be estimated to few percent of the overall intensity. Considering the logarithmic scale in Fig. 4, the limited dynamic range of the high-speed camera (10 bit) has to be considered. Although it can be neglected for higher densities and is acceptable between about 4 and 7.5 ms, the detected signals are rather low compared to the noise level before and after this time. The densities before 4 ms can have uncertainties of more than 100 %. Nevertheless the information about the rise of density and the order of magnitude is valuable.

4. Summary and outlook

In this work, the radial and axial distributions of atomic and ionic lines during transitions from diffuse mode to different high-current modes are investigated. During transition from anode spot type 1 to anode spot type 2 an abrupt change appears in the arc voltage and in both intensities near the anode and cathode.

The determined radial distributions of radiating densities of the Cu I and Cu II lines show that the radiating density of the atomic line is higher than that of the ionic line during anode spot modes. In addition, the atomic radiating density during anode spot type 2 is 5 times higher than during anode spot type 1. The density of the Cu III line outside the high intensity shell of the anode spot is higher than that of Cu II.

Determining the ground state density and temperature during different high current anode modes is scheduled as a future work considering the non-equilibrium vacuum arc plasma.

References

[1] E Schade and E Dullni. Recovery of breakdown strength of a vacuum interrupter after extinction of high current. *IEEE Trans. Dielectr. Elect. Insul.*, 9(2):207–215, 2002. doi:10.1109/94.993737.

[2] E. Dullni and E. Schade. Investigation of high-current interruption of vacuum circuit breakers. *IEEE Trans. Dielectr. Elect. Insul.*, 28(4):607–620, 1993. doi:10.1109/14.231543.

[3] H. C. Miller. A review of anode phenomena in vacuum arcs. *Contrib. Plasma Phys.*, 29(3):223–249, 1989. doi:10.1109/TPS.1985.4316413.

[4] A. Khakpour et al. Video spectroscopy of vacuum arcs during transition between different high-current anode modes. *IEEE Trans. Plasma Sci.*, 44(10):2462–2469, 2016. doi:10.1109/TPS.2016.2602384.

[5] A. Khakpour et al. Optical and electrical investigation of transition from anode spot type 1 to anode spot type 2. *IEEE Trans. Plasma Sci.*, 45(8):2126–2134, 2017. doi:10.1109/TPS.2017.2690572.

[6] P. G. Slade. *The Vacuum Interrupter: Theory, Design, and Application.* Boca Raton, FL, USA: CRC Press, 2008.